Geochemical Perspectives Letters

© 2017 European Association of Geochemistry

Late accretion history of the terrestrial planets inferred from platinum stable isotopes

J.B. Creech[1,2]*, J.A. Baker[3], M.R. Handler[4], J.-P. Lorand[5], M. Storey[6], A.N. Wainwright[7], A. Luguet[8], F. Moynier[2,9], M. Bizzarro[1]

OPEN ACCESS

Abstract

doi: 10.7185/geochemlet.1710

Late accretion of chondritic material to differentiated planetary bodies is thought to have been common in the early solar system. However, the timing and scale of admixing this material to terrestrial planets are poorly constrained. Using platinum (Pt) stable isotope data in a range of solar system bodies, we show that Earth's post-Archean mantle has chondritic $^{198}Pt/^{194}Pt$, consistent with addition of a chondritic late-veneer after core formation. Conversely, terrestrial Archean samples record non-chondritic, heavy, $^{198}Pt/^{194}Pt$, indicating preservation of early mantle components that escaped complete mixing with the late-veneer. These data suggest admixing of ≤50 % of the eventual full late-veneer inventory. Such effective mixing within Earth's mantle by 3.85 Ga is most consistent with modern-style plate tectonics.

Received 7 September 2016 | Accepted 19 October 2016 | Published 8 November 2016

1. Centre for Star and Planet Formation, Natural History Museum of Denmark, University of Copenhagen, Øster Voldgade 5-7, 1350 Copenhagen, Denmark
2. Institut de Physique du Globe de Paris, Université Sorbonne Paris Cité, Université Paris Diderot, 1 Rue Jussieu, 75328 Paris Cedex 05, France
* Corresponding author (email: creech@ipgp.fr)
3. School of Environment, The University of Auckland, Private Bag 92019, Auckland, New Zealand
4. School of Geography, Environment and Earth Sciences, Victoria University of Wellington, PO Box 600, Wellington, New Zealand
5. Laboratoire de Planétologie et Géodynamique de Nantes, CNRS UMR 6112, Université de Nantes, 2 Rue de la Houssinière, BP 92208, 44322 Nantes Cedex 3, France
6. Quadlab, Natural History Museum of Denmark, University of Copenhagen, Øster Voldgade 5-7, 1350 Copenhagen, Denmark
7. Laboratoire G-Time, Université Libre de Bruxelles, 50 Avenue F.D. Roosevelt, 1050 Brussels, Belgium
8. Steinmann Institut für Geologie Mineralogie und Paläontologie, Rheinische Friedrich-Wilhems-Universität, 53115 Bonn, Germany
9. Institut Universitaire de France, 75005 Paris, France

Letter

Cratering of the lunar surface provides evidence for a cataclysmic late bombardment event that culminated 3.9 Gyr ago, possibly associated with the disturbance of the planetesimal disk triggered by migration of the gas giants (Gomes *et al.*, 2005). The late-veneer refers to the sum of material added to Earth's mantle after the final episode of core formation, which is thought to have comprised a contribution of ~0.5 wt. % of Earth's mass (~2 $\times 10^{22}$ kg) from chondritic material (Walker, 2009). Addition of this material can explain the elevated mantle HSE abundances and their broadly chondritic relative proportions (Lorand *et al.*, 2008; Walker, 2009), and provide a mechanism for the delivery of volatiles to Earth (Owen and Bar-Nun, 1995). Alternatively, due to changes in partitioning behaviour of HSE under different physical conditions, the elevated HSE abundances in Earth's mantle may be the result of core formation at high-temperatures and -pressures (Mann *et al.*, 2012). The late-veneer hypothesis is apparently supported by the existence of small enrichments in ^{182}W in the early Archean terrestrial rock record (Willbold *et al.*, 2011, 2015; Touboul *et al.*, 2014). However, the timing and scale of veneering of the early Earth are poorly constrained and the origin of these Archean enrichments is controversial (*e.g.*, Rizo *et al.*, 2016). Moreover, the utility of the ^{182}W tracer is limited to young planetary bodies, as late accretion signatures may be overprinted from radiogenic ingrowth from the decay of the short-lived ^{182}Hf nuclide ($t_{1/2}$ = 8.9 Myr) in early-formed bodies.

We developed the techniques for the investigation of natural stable isotope fractionation of the HSE platinum (Creech *et al.*, 2013, 2014), which is a novel tool to investigate the late accretion history of the terrestrial planets. Stable isotopic fractionations relating to metal–silicate differentiation have been reported in several stable isotope systems, *e.g.*, Si (Young *et al.*, 2015), Mo (Hin *et al.*, 2013; Burkhardt *et al.*, 2014), Zn (Mahan *et al.*, 2017). The metal–silicate partitioning of Pt is much greater than for these other elements and, combined with the differences in oxidation state and bonding environment between mantle silicates and the Fe–Ni metallic core, Pt has the potential for significant stable isotope fractionation related to metal–silicate partitioning and core formation. Theory predicts that the heavy isotopes of an element will tend to be concentrated in the most oxidised component of a system (Schauble, 2004), which is supported by experimental data for Mo (Hin *et al.*, 2013), and therefore heavy Pt stable isotopes might be expected in oxidised silicate mantles of differentiated bodies. Here, we present Pt stable isotope data for major solar system reservoirs, including chondrites, achondrites and Earth, to trace late accretion processes.

Platinum isotope data are expressed in $\delta^{198}Pt$ notation, which reports per mil (‰) deviations in the $^{198}Pt/^{194}Pt$ ratio relative to a standard, corrected for instrumental fractionation using a ^{196}Pt–^{198}Pt double spike. The double-spike correction assumes that there are no mass-independent fractionation effects arising from nucleosynthetic processes. Nucleosynthetic variability has been documented in relatively low mass siderophile elements, such as Mo and Ru, with significant nucleosynthetic isotope heterogeneity existing between the various

classes of chondrites (*e.g.*, Burkhardt *et al.*, 2011; Fischer-Gödde *et al.*, 2015). However, so far no isotopic anomalies have been documented in heavy siderophile elements with masses more comparable to Pt (*e.g.*, Os, Te, Cd; Yokoyama and Walker, 2016). If variations on a similar scale to those in Mo and Ru exist for Pt, we would expect to see large variations in double-spike data corrected assuming mass dependent fractionation, particularly between chondrite groups.

We determined the δ^{198}Pt values of chondrites, as these are thought to represent the bulk composition of the solar system and the putative veneering material. Platinum stable isotope compositions of chondrites are identical across groups (ordinary, enstatite and carbonaceous), establishing Pt stable isotope homogeneity amongst primitive solar system bodies. This observation confirms that nucleosynthetic variations in Pt, if present, must be very limited and well within the uncertainties of our measurements. In contrast to enstatite and ordinary chondrites, carbonaceous chondrites contain significant amounts of refractory inclusions, which are known to preserve nucleosynthetic anomalies for a number of elements (Birck, 2004). Combined with the relatively small sample size (<0.5 g) of many of the carbonaceous chondrites analysed, this may explain the greater variability in this group (see Supplementary Information for further discussion). As such, we use enstatite and ordinary chondrites as well as replicates from a ~15 g aliquot of the Allende carbonaceous chondrite to define the chondritic δ^{198}Pt = –0.14 ± 0.03 ‰ (2 sd).

We investigate the effect of metal–silicate differentiation on Pt stable isotopes using achondrite meteorites. Primitive achondrites sample bodies that have undergone varying degrees of metal–silicate segregation, as reflected by HSE abundances that span a range from ~50–1500 ng g^{-1} (Warren *et al.*, 2006; Rankenburg *et al.*, 2008) which has been interpreted to reflect the early stages of core formation (Warren *et al.*, 2006). The primitive achondrites show increasingly heavy δ^{198}Pt from chondritic values to ≥0.35 ‰ heavier than chondrites with decreasing HSE content (Fig. 1). We interpret this to reflect Pt stable isotopic fractionation during core formation, whereby the heavy isotopes of Pt are preferentially retained in the more oxidised silicate part of the body while the light isotopes are concentrated in the metallic core, which is consistent with qualitative predictions based on stable isotope theory (Schauble, 2004) and Mo experimental data (Hin *et al.*, 2013) as described above. Given the leverage of the metallic core, which contains >99.99 % of the Pt, the greatest fractionation is observed in the most Pt depleted primitive achondrite samples (Fig. 1). However, as these represent relatively small degrees of metal–silicate differentiation, the magnitude of heavy Pt isotope enrichment provides only a minimum constraint on the Pt stable isotopic fractionation during core formation. In contrast, iron meteorites represent the cores of their respective parent bodies and have very high HSE abundances and chondritic Pt stable isotope composition (δ^{198}Pt = –0.19 ± 0.11 ‰; Fig. 1). We note that larger uncertainties in iron meteorite data potentially arise from cosmogenic effects, as discussed in the Supplementary Information.

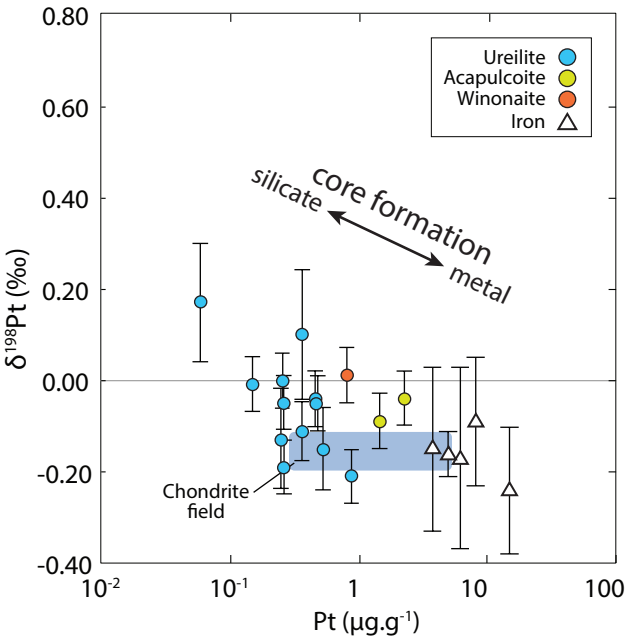

Figure 1 Platinum stable isotopes *vs.* Pt concentrations in achondrite meteorite samples showing increasingly heavy Pt isotopic compositions corresponding with decreasing Pt concentrations, indicating that heavy Pt isotopes are concentrated in the silicate mantle during metal–silicate differentiation. The shaded field represents the mean and 2 sd of chondrites, as given in the text. Error bars on δ^{198}Pt are the 2 sd of combined measurements or the reproducibility of the method as determined by replicate digestions of similar samples, whichever is larger (Supplementary Information). Uncertainties in Pt concentration are negligible on this logarithmic scale. Iron meteorite samples have larger uncertainties in δ^{198}Pt owing to cosmogenic effects, which are discussed further in the Supplementary Information. A regression through the ureilite data gives a slope of –0.108 ‰ per log unit of concentration (r^2 ~0.43); excluding ALHA81101, the slope is 0.069 ‰ per log unit of concentration, (r^2 ~0.14).

The post-Archean terrestrial mantle, represented by mantle peridotites sampled from various geological settings and localities (Table S-1), has a mean δ^{198}Pt of –0.10 ± 0.10 ‰ (2 sd; Fig. 2), which is indistinguishable from the chondritic value. There is some variability amongst post-Archean mantle xenolith samples, possibly reflecting mantle processes such as melt extraction or metasomatism, but the limited range suggests that the Pt stable isotope composition of Earth's convecting mantle has been homogeneous since the Proterozoic. The absence of a heavy Pt stable isotopic signature in Earth's post-Archean mantle suggests that the isotopic signature of core formation on Earth has been overprinted by a late-veneer of chondritic material, although it is not possible to constrain which type of chondrite may have dominated the late accreted material.

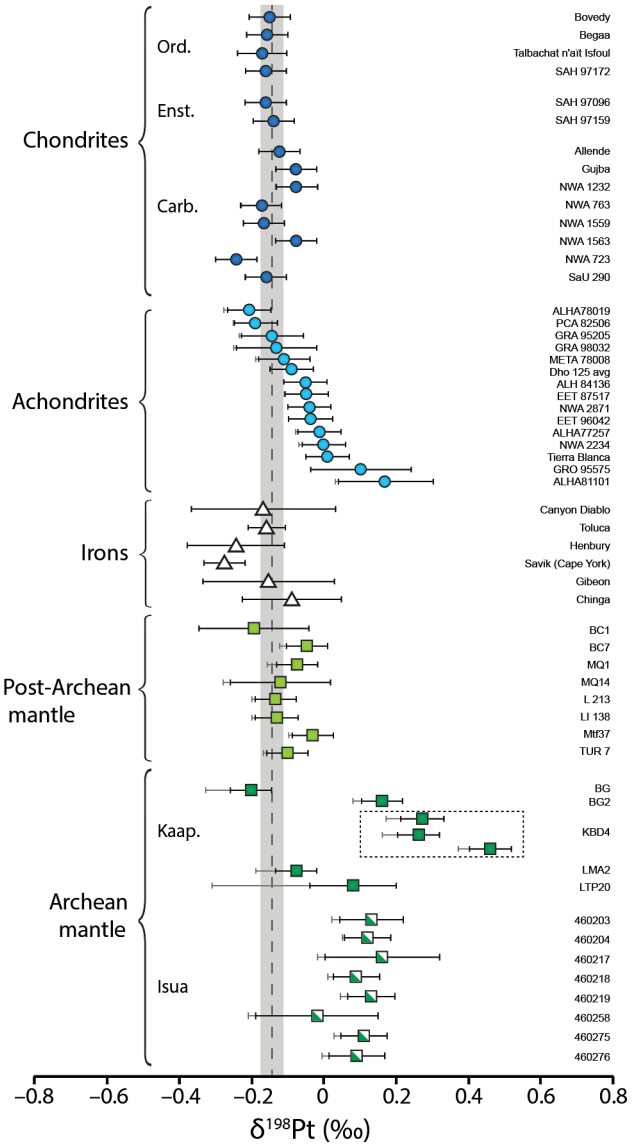

Figure 2 Platinum stable isotope results for terrestrial and meteorite samples. Error bars on δ^{198}Pt for NiS digested samples are the 2 sd of combined replicates or the reproducibility of the method as determined by replicate digestions of similar samples, whichever is larger (Supplementary Information). Extended error bars illustrate the additional uncertainty arising from the potential presence of small amounts of analytical blank (further details are given in the Supplementary Information). The dashed vertical line and grey box represent the mean and 2 sd of chondrites as discussed in the text. For one Kaapvaal sample where the variability in replicate digestions exceeded the reproducibility of the technique (interpreted as reflecting real isotopic heterogeneity on the scale of these samples) all three replicates are shown enclosed in a dashed box, where the size of the box represents the 2 sd of the three replicates. Large uncertainties on iron meteorite samples are attributed to cosmic ray exposure effects, which are expected to shift δ^{198}Pt to more negative values; further discussion is given in the Supplementary Information.

In contrast to post-Archean mantle, Archean terrestrial rocks from southern Africa and Greenland have non-chondritic, heavy Pt stable isotopes. The cratonic xenolith suite from southern Africa, sampled from Kaapvaal craton kimberlites, have δ^{198}Pt extending to significantly (≥0.5 ‰) heavier compositions than chondrites and post-Archean mantle (Fig. 2). Kimberlite-hosted peridotite xenoliths from this area are considered to represent sub-cratonic lithospheric mantle up to 3.6 Ga in age (Griffin *et al.*, 2004), and all five samples have Late Archean Os model ages (Table S-1). While depletions in incompatible PGE (Pd, Pt, Re; Table S-1) indicate extraction of partial melts, the low Pt concentrations (0.4–2.7 ng g^{-1}) in these samples relative to our post-Archean mantle xenoliths (5.2–7.3 ng g^{-1}) could also be consistent with a smaller late-veneer Pt contribution in the Kaapvaal subcratonic mantle. Variable HSE concentrations in kimberlite-hosted xenoliths have been interpreted to represent the sluggish equilibration of Archean mantle with the putative late-veneer (Maier *et al.*, 2012), in keeping with the Pt stable isotopic variability in these samples. We also find that metabasalts and ultramafic schists from the >3.85 Ga (Nutman *et al.*, 1997) Isua Supracrustal Belt also have heavy δ^{198}Pt (Fig. 2). Given the large degrees of partial melting required to produce the Isua rocks (based on high-MgO content), the Pt concentrations and isotope compositions of these samples likely reflect their mantle source. Moreover, these samples also preserve ^{142}Nd excesses of up to ~10 ppm from the decay of short-lived ^{146}Sm ($t_{1/2}$ ~ 68–103 Ma), indicative of the early differentiation of their source reservoir (Rizo *et al.*, 2013). The heavy Pt stable isotopic compositions observed in these geographically separated Archean rocks from Africa and Greenland are not found in any younger mantle samples analysed thus far. Given the fractionation towards heavier δ^{198}Pt in the silicate component during core formation inferred from achondrites, we interpret the heavy Pt isotopic compositions in these Archean samples as reflecting preservation of a pre-late-veneer signature of Earth's core formation. This is consistent with ^{182}W data from Isua and other ancient rocks (Willbold *et al.*, 2011, 2015; Touboul *et al.*, 2014), which have also been interpreted to reflect long-term preservation of pre-late-veneer mantle that had escaped complete mixing with late-veneer.

Although both sets of Archean samples have lower Pt concentrations than post-Archean samples (Table S-1), Pt is not as depleted as would be expected for pre-late-veneer material under low-pressure and -temperature core-forming conditions. Experimentally determined HSE partition coefficients at

high-pressures and -temperatures cannot explain mantle abundances by equilibrium core formation alone (Mann *et al.*, 2012). However, if the core formed under these conditions, the Pt depletion in the pre-late-veneer mantle would be significantly reduced (*e.g.*, Pt ~ 0.1 ng g^{-1} in pre-late-veneer mantle as compared with *ca.* 7 ng g^{-1} in the primitive upper mantle; Becker *et al.*, 2006), and a combination of high-pressure and -temperature core formation with a chondritic late-veneer can explain both the Pt concentrations and Pt stable isotope data. Mixing calculations modelling the effect of addition of chondritic late-veneer (with δ^{198}Pt ~ –0.14 ‰ and 1 µg g^{-1} Pt) to a hypothetical pre-late-veneer mantle can reproduce our Pt isotope and concentration data for Isua and post-Archean mantle if we assume a pre-late-veneer mantle with 0.14 ng g^{-1} Pt (using partition coefficients for core formation at high-pressure and -temperature), Pt isotopic fractionation during core formation of ~4 ‰, and a final amount of late-veneer equating to 0.5 wt.% of Earth's mass (Fig. 3; Supplementary Information). Based on this, the Pt abundance in Isua samples can be interpreted as reflecting admixing of up to ~50 % of the full complement of late-veneer (Fig. 3), which is consistent with recent ^{182}W data indicating that the lunar mantle has a marginally greater ^{182}W enrichment relative to the early Archean terrestrial mantle (Kruijer *et al.*, 2015; Touboul *et al.*, 2015).

The Kaapvaal peridotite xenoliths have approximately half the Pt content of the Isua samples, although the variable Pt concentrations and isotopic compositions likely reflect variable degrees of equilibration with the kimberlite host and/or post-veneer convecting mantle. Thus, the heaviest isotopic composition, defined by multiple digestions of the sample KBD-4 (δ^{198}Pt = 0.27–0.46 ‰), is considered to represent the most pristine pre-late-veneer signature. The heavier δ^{198}Pt and lower Pt concentrations of the Kaapvaal mantle xenoliths could indicate that they preserve a more pristine pre-late-veneer signature relative to Isua, which may reflect an older mantle source or, alternatively, spatial heterogeneity. These observations require that progressive admixing of veneering material to Earth's mantle was initiated prior to the formation of the Isua mantle source at ≥4.3 Ga based on the ^{146}Sm–^{142}Nd decay system (Rizo *et al.*, 2013). Accepting an age of ~4.4 Ga for the timing of the Moon-forming impact (Borg *et al.*, 2011), our data suggest that the delivery, admixing, and homogenisation of chondritic, perhaps volatile-rich, material to the early Earth occurred very shortly after magma ocean crystallisation. This requires efficient mixing of the Hadean mantle, which is most easily understood in the framework of modern-style, mobile-lid tectonics rather than a stagnant-lid regime (Debaille *et al.*, 2013). More speculatively, the early delivery of volatile-rich material through impact may have promoted rapid formation of the terrestrial hydrosphere and, hence, assisted hydration of the crust that is required for the inception of plate tectonic processes (O'Neill *et al.*, 2007).

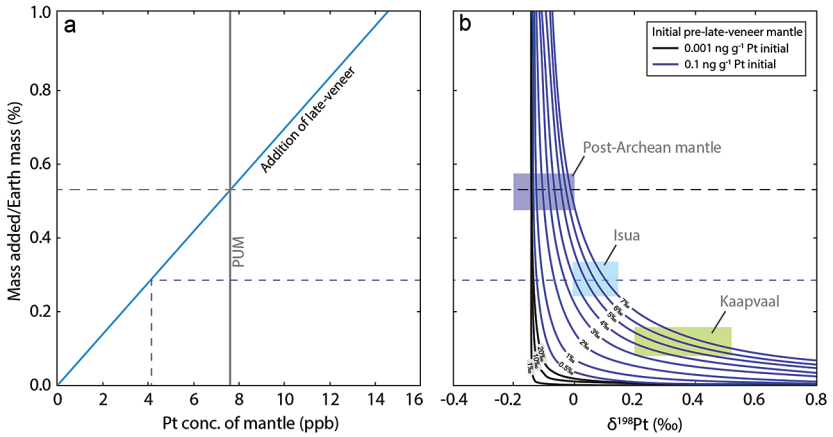

Figure 3 Model of the effect of addition of chondritic late-veneer on the abundance and isotopic composition of Pt in the mantle. (a) The calculated mantle concentration of Pt from the addition of chondrite to the pre-late-veneer mantle. The vertical line represents the Pt concentration of primitive upper mantle (PUM; 7.6 ppb; Becker *et al.*, 2006), and the dashed horizontal line marks the intercept of the mantle concentration with PUM, indicating the amount of late-veneer required to reproduce the Pt abundance of PUM. (b) The Pt isotopic composition of the mantle resulting from mixing late-veneer with hypothetical pre-late-veneer mantle, with black and blue lines representing mixtures with initial pre-late-veneer mantle Pt concentrations of ≤0.001 ng g^{-1} and 0.144 ng g^{-1}, relating to core formation at low- or high-pressures and -temperatures, respectively (Supplementary Information). Shaded boxes represent the composition of the post-Archean mantle and inferred composition of the Archean mantle sources of Isua and Kaapvaal (based on the range of values defined by the sample KBD4, which is taken to represent the most pristine pre-late-veneer signature). Note that the latter was not used to constrain the model, as Pt concentrations may not relate solely to depletion during core-formation.

Acknowledgements

The authors wish to thank Henning Haack for providing the sample Savik, NASA for providing ureilite meteorite samples, Minik Rosing at the Natural History Museum of Denmark and Tod Waight at IGN, Copenhagen University for use of rock powdering facilities, and Rosemary Arts for help in the laboratory. This research was supported by a Royal Society of New Zealand Marsden Grant to MH and JB and grants from the Danish National Research Foundation (grant number DNRF97) and from the European Research Council (ERC Consolidator grant agreement 616027-STARDUST2ASTEROIDS) to M.B. F.M. acknowledges funding from the European Research Council (ERC Starting grant agreement 637503-Pristine) as well as the financial support of the UnivEarthS Labex program at Sorbonne Paris Cité (ANR-10-LABX-0023 and ANR-11-IDEX-0005-02) and a *chaire d'excellence* ANR-Idex Sorbonne Paris Cité. AL and AW thank Kevin Burton

and Geoff Nowell (Earth Science Department, University Durham, UK) for the Os contents and $^{187}Os/^{188}Os$ compositions determination of the Kaapvaal cratonic peridotites. All data are available in the main manuscript and Supplementary Information. We also thank Pierre Olivier Foucault and Joel Dyon (IPGP) for producing the image for the graphical abstract.

Editor: Helen Williams

Additional Information

Supplementary Information accompanies this letter at www.geochemicalperspectivesletters.org/article1710

Reprints and permission information are available online at http://www.geochemicalperspectivesletters.org/copyright-and-permissions

Cite this letter as: Creech, J.B., Baker, J.A., Handler, M.R., Lorand, J.-P., Storey, M., Wainwright, A.N., Luguet, A., Moynier, F., Bizzarro, M. (2017) Late accretion history of the terrestrial planets inferred from platinum stable isotopes. *Geochem. Persp. Let.* 3, 94–104.

References

Becker, H., Horan, M.F., Walker, R.J., Gao, S., Lorand, J.-P., Rudnick, R.L. (2006) Highly siderophile element composition of the Earth's primitive upper mantle: Constraints from new data on peridotite massifs and xenoliths. *Geochimica et Cosmochimica Acta* 70, 4528–4550.

Birck, J.L. (2004) An Overview of Isotopic Anomalies in Extraterrestrial Materials and Their Nucleosynthetic Heritage. *Reviews in Mineralogy and Geochemistry* 55, 25–64.

Borg, L.E., Connelly, J.N., Boyet, M., Carlson, R.W. (2011) Chronological evidence that the Moon is either young or did not have a global magma ocean. *Nature* 477, 70–72.

Burkhardt, C., Kleine, T., Oberli, F., Pack, A., Bourdon, B., Wieler, R. (2011) Molybdenum isotope anomalies in meteorites: Constraints on solar nebula evolution and origin of the Earth. *Earth and Planetary Science Letters* 312, 390–400.

Burkhardt, C., Hin, R.C., Kleine, T., Bourdon, B. (2014) Evidence for Mo isotope fractionation in the solar nebula and during planetary differentiation. *Earth and Planetary Science Letters* 391, 201–211.

Creech, J., Baker, J., Handler, M., Schiller, M., Bizzarro, M. (2013) Platinum stable isotope ratio measurements by double-spike multiple collector ICPMS. *Journal of Analytical Atomic Spectrometry* 28, 853–865.

Creech, J.B., Baker, J.A., Handler, M.R., Bizzarro, M. (2014) Platinum stable isotope analysis of geological standard reference materials by double-spike MC-ICPMS. *Chemical Geology* 363, 293–300.

Debaille, V., O'Neill, C., Brandon, A.D., Haenecour, P., Yin, Q.-Z., Mattielli, N., Treiman, A.H. (2013) Stagnant-lid tectonics in early Earth revealed by ^{142}Nd variations in late Archean rocks. *Earth and Planetary Science Letters* 373, 83–92.

Fischer-Gödde, M., Burkhardt, C., Kruijer, T.S., Kleine, T. (2015) Ru isotope heterogeneity in the solar protoplanetary disk. *Geochimica et Cosmochimica Acta* 168, 151–171.

Gomes, R., Levison, H.F., Tsiganis, K., Morbidelli, A. (2005) Origin of the cataclysmic Late Heavy Bombardment period of the terrestrial planets. *Nature* 435, 466–469.

Griffin, W.L., Graham, S., O'Reilly, S.Y., Pearson, N.J. (2004) Lithosphere evolution beneath the Kaapvaal Craton: Re–Os systematics of sulfides in mantle-derived peridotites. *Chemical Geology* 208, 89–118.

Hin, R.C., Burkhardt, C., Schmidt, M.W., Bourdon, B., Kleine, T. (2013) Experimental evidence for Mo isotope fractionation between metal and silicate liquids. *Earth and Planetary Science Letters* 379, 38–48.

Kruijer, T.S., Kleine, T., Fischer-Gödde, M., Sprung, P. (2015) Lunar tungsten isotopic evidence for the late veneer. *Nature* 520, 534–537.

Lorand, J.-P., Luguet, A., Alard, O. (2008) Platinum-Group Elements: A New Set of Key Tracers for the Earth's Interior. *Elements* 4, 247–252.

Mahan, B., Siebert, J., Pringle, E.A., Moynier, F. (2017) Elemental partitioning and isotopic fractionation of Zn between metal and silicate and geochemical estimation of the S content of the Earth's core. *Geochimica et Cosmochimica Acta* 196, 252–270.

Maier, W.D., Peltonen, P., McDonald, I., Barnes, S.J., Barnes, S.-J., Hatton, C., Viljoen, F. (2012) The concentration of platinum-group elements and gold in southern African and Karelian kimberlite-hosted mantle xenoliths: Implications for the noble metal content of the Earth's mantle. *Chemical Geology* 302–303, 119–135.

Mann, U., Frost, D.J., Rubie, D.C., Becker, H., Audétat, A. (2012) Partitioning of Ru, Rh, Pd, Re, Ir and Pt between liquid metal and silicate at high pressures and high temperatures - Implications for the origin of highly siderophile element concentrations in the Earth's mantle. *Geochimica et Cosmochimica Acta* 84, 593–613.

Nutman, A.P., Mojzsis, S.J., Friend, C.R.L. (1997) Recognition of ≥3850 Ma water-lain sediments in West Greenland and their significance for the early Archaean Earth. *Geochimica et Cosmochimica Acta* 61, 2475–2484.

O'Neill, C., Jellinek, A.M., Lenardic, A. (2007) Conditions for the onset of plate tectonics on terrestrial planets and moons. *Earth and Planetary Science Letters* 261, 20–32.

Owen, T., Bar-Nun, A. (1995) Comets, impacts, and atmospheres. *Icarus* 116, 215–226.

Rankenburg, K., Humayun, M., Brandon, A.D., Herrin, J.S. (2008) Highly siderophile elements in ureilites. *Geochimica et Cosmochimica Acta* 72, 4642–4659.

Rizo, H., Boyet, M., Blichert-Toft, J., Rosing, M.T. (2013) Early mantle dynamics inferred from ^{142}Nd variations in Archean rocks from southwest Greenland. *Earth and Planetary Science Letters* 377, 324–335.

Rizo, H., Walker, R.J., Carlson, R.W., Touboul, M., Horan, M.F., Puchtel, I.S., Boyet, M., Rosing, M.T. (2016) Early Earth differentiation investigated through ^{142}Nd, ^{182}W, and highly siderophile element abundances in samples from Isua, Greenland. *Geochimica et Cosmochimica Acta* 175, 319–336.

Schauble, E.A. (2004) Applying Stable Isotope Fractionation Theory to New Systems. *Reviews in Mineralogy and Geochemistry* 55, 65–111.

Touboul, M., Liu, J., O'Neil, J., Puchtel, I.S., Walker, R.J. (2014) New insights into the Hadean mantle revealed by ^{182}W and highly siderophile element abundances of supracrustal rocks from the Nuvvuagittuq Greenstone Belt, Quebec, Canada. *Chemical Geology* 383, 63–75.

Touboul, M., Puchtel, I.S., Walker, R.J. (2015) Tungsten isotopic evidence for disproportional late accretion to the Earth and Moon. *Nature* 520, doi: 10.1038/nature14355.

Walker, R.J. (2009) Highly siderophile elements in the Earth, Moon and Mars: Update and implications for planetary accretion and differentiation. *Chemie der Erde - Geochemistry* 69, 101–125.

Warren, P.H., Ulff-Møller, F., Huber, H., Kallemeyn, G.W. (2006) Siderophile geochemistry of ureilites: A record of early stages of planetesimal core formation. *Geochimica et Cosmochimica Acta* 70, 2104–2126.

Willbold, M., Elliott, T., Moorbath, S. (2011) The tungsten isotopic composition of the Earth's mantle before the terminal bombardment. *Nature* 477, 195–198.

Willbold, M., Mojzsis, S.J., Chen, H.-W., Elliott, T. (2015) Tungsten isotope composition of the Acasta Gneiss Complex. *Earth and Planetary Science Letters* 419, 168–177.

Yokoyama, T., Walker, R.J. (2016) Nucleosynthetic Isotope Variations of Siderophile and Chalcophile Elements in the Solar System. *Reviews in Mineralogy and Geochemistry* 81, 107–160.

Young, E.D., Manning, C.E., Schauble, E.A., Shahar, A., Macris, C.A., Lazar, C., Jordan, M. (2015) High-temperature equilibrium isotope fractionation of non-traditional stable isotopes: Experiments, theory, and applications. *Chemical Geology* 395, 176–195.

Late accretion history of the terrestrial planets inferred from platinum stable isotopes

J.B. Creech[1,2]*, J.A. Baker[3], M.R. Handler[4], J.-P. Lorand[5], M. Storey[6], A.N. Wainwright[7], A. Luguet[8], F. Moynier[2,9], M. Bizzarro[1]

Supplementary Information

This supplementary information includes:

- Materials and Methods
- Supplementary Text
- Figures S-1 and S-2
- Tables S-1 to S-8
- Supplementary Information References

1. Centre for Star and Planet Formation, Natural History Museum of Denmark, University of Copenhagen, Øster Voldgade 5-7, 1350 Copenhagen, Denmark
2. Institut de Physique du Globe de Paris, Université Sorbonne Paris Cité, Université Paris Diderot, 1 Rue Jussieu, 75328 Paris Cedex 05, France
* Corresponding author (email: creech@ipgp.fr)
3. School of Environment, The University of Auckland, Private Bag 92019, Auckland, New Zealand
4. School of Geography, Environment and Earth Sciences, Victoria University of Wellington, PO Box 600, Wellington, New Zealand
5. Laboratoire de Planétologie et Géodynamique de Nantes, CNRS UMR 6112, Université de Nantes, 2 Rue de la Houssinière, BP 92208, 44322 Nantes Cedex 3, France
6. Quadlab, Natural History Museum of Denmark, University of Copenhagen, Øster Voldgade 5-7, 1350 Copenhagen, Denmark
7. Laboratoire G-Time, Université Libre de Bruxelles, 50 Avenue F.D. Roosevelt, 1050 Brussels, Belgium
8. Steinmann Institut für Geologie Mineralogie und Paläontologie, Rheinische Friedrich-Wilhems-Universität, 53115 Bonn, Germany
9. Institut Universitaire de France, 75005 Paris, France

Materials and Methods

The techniques utilised in this study for Pt are described in detail in earlier work (Creech *et al.*, 2013, 2014; Creech and Paul, 2015). All sample preparation, digestions and chemical separations were carried out in ultra-clean laboratory conditions at either Victoria University of Wellington, New Zealand, the Centre for Star and Planet Formation, Natural History Museum of Denmark, or at the Institut de Physique du Globe de Paris, France.

Sample information

1. Terrestrial samples. Terrestrial sample information is summarised in Table S-1. Sample masses for peridotite samples were typically 15 g. However, depending on the amount of sample available, some samples were as small as *ca*. 7 g or as much as *ca*. 45 g (processed as multiple replicates).

Four peridotite mantle xenolith samples from northern Queensland, Australia were analysed in this study. BC1 and BC7 are from Batchelor's Crater, which is a Plio–Pleistocene alkali basalt vent in the Chudleigh volcanic province. MQ1 and MQ14 are from Mount Quincan in the <3 Ma Atherton Tablelands volcanic province. Major and trace element and Sm–Nd isotopic data for a suite of peridotite xenoliths from this locality, including both of these samples, were presented by Handler *et al*. (2005). The Mount Quincan xenolith suite represent a fertile mantle source with a ^{147}Sm–^{143}Nd age of *ca*. 275 Ma (Handler *et al.*, 2005).

Two ophiolite/transitional lherzolite samples emplaced during the Mesozoic rifting of the Italian Alps were measured in this study. LI 138 is from the Internal Liguride Ophiolite (Luguet *et al.*, 2004). L 213 from the Sezia Lanzo HP zone is a spinel/plagioclase lherzolite from the northern part of the Lanzo lherzolite massif that represents fragment of a continental lithosphere that accreted during the early Palaeozoic/late Proterozoic (Bodinier *et al.*, 1991). Mtf37 is an off-craton, basalt-hosted highly fertile lherzolite xenolith from Montferrier, southern Massif Central, France (Alard *et al.*, 2011). TUR 7 is a highly fertile continental orogenic lherzolite from Turon de Técouère, Pyrenees, France (Fabriès *et al.*, 1998). All four samples are LREE-depleted lherzolites showing little evidence of secondary cryptic/modal metasomatism and variable serpentinisation (close to 0 % in TUR 7 and Mtf37, 20 % for LI 138 and close to 100 % for LI 138).

Five cratonic xenoliths from southern Africa were analysed in this study. All five samples have late Archean Os model ages (Table S-1). LMA2 and LTP20 are xenoliths from the Matsoku and Thaba Putsoa kimberlites, respectively, in Lesotho. KBD4, BG and BG2 xenoliths come from diamondiferous kimberlite pipes of the Kimberley area, South Africa. KBD4 and BG2 are described as harzburgitic, whereas BG is lherzolitic (Lorand and Grégoire, 2006). The cratonic xenoliths are characterised by lower Pt concentrations (0.4–2.7 ng g^{-1}; Table S-1) than other mantle samples analysed in this study.

Eight rocks from the Isua Supracrustal Belt were analysed. A lithologically diverse package of early Archean supracrustal rocks occurs in a ~5 km wide arcuate belt at Isua, Southwest Greenland. In the southwest part of the belt, pillow lava structures are recognised within low deformation zone windows within a sequence of amphibolite rocks. Compositionally, the pillows are high-MgO (12–15 wt. %) tholeiitic basalts and are associated with ultramafic schists of komatiitic composition. A felsic unit which cross-cuts this pillow lava-bearing sequence gives U-Pb SHRIMP ages clustering around ~3.85 Ga (Baadsgaard *et al.*, 1984; Michard-Vitrac *et al.*, 1977; Nutman *et al.*, 1997) suggesting that these amphibolites are amongst the oldest of the Isua supracrustals. Ultramafic schists occur as scattered outcrops within the general vicinity of the pillow basalts and have compositions typical of Archean komatiites (*ca*. 25–27 wt. % MgO), and therefore most likely represent very high degree melts. We analysed six samples from the metabasalts, as well as two samples from the ultramafic schists (Table S-1). High-precision Nd isotope data have been previously reported for five of the Isua samples analysed here (Rizo *et al.*, 2013), and major and trace element data for these samples are also provided in that work.

2. Meteorite samples. Meteorite sample information is summarised in Table S-2. A total of 40 meteorite samples were analysed in this study. The 14 chondrites samples comprise four ordinary chondrites, two enstatite chondrites and eight carbonaceous chondrites. The 15 primitive achondrites analysed comprise two acapulcoites, one winonaite and 12 ureilites, of which 11 are Antarctic meteorites provided by NASA-JSC. The six iron meteorites analysed comprise two IAB, two IIIAB, one IVA and one IVB.

For most meteorite samples, typical sample sizes were *ca.* 0.5–1.0 g (Table S-2). For one of the carbonaceous chondrites (Allende), a large fragment (~15 g) was crushed and homogenised with an agate mortar and pestle, from which five replicate digestions of *ca.* 1 g were each processed to assess the reproducibility of the technique (Table S-2). Previously published cosmic ray exposure (CRE) ages for the iron meteorites are also given in Table S-2, although no correlation between Pt isotopes and CRE ages was observed. Further details about the meteorites analysed can be obtained from the Meteoritical Bulletin Database (http://www.lpi.usra.edu/meteor/).

Sample preparation and digestion (Pt)

Digestions of chondrite, primitive achondrite and terrestrial samples were carried out using a NiS fire assay method as described by Creech *et al.* (2014). All sample powdering was carried out using agate mortar and pestle or agate mills. Powders were weighed directly into porcelain crucibles for NiS digestion. Prior to powdering, fragments of chondrite and achondrite meteorites were taken from sliced specimens, weighed and then cleaned by rinsing in ultra-pure water, methanol and again in ultra-pure water. The meteorite fragments, typically weighing 0.5–1.0 g, were then placed in a Savillex teflon beaker in *ca*. 4 mL of

2 M HCl. The beakers were heated to 120 ˚C for *ca.* 10 min and then ultrasonicated for *ca*. 3 min. After this gentle acid washing, the samples were rinsed twice with water and then dried in the beaker on a hotplate before crushing and transferring to porcelain crucibles for NiS fire assay digestion. Samples were double-spiked prior to NiS digestion by adding the ^{196}Pt–^{198}Pt double-spike (DS) directly to the mixture in the crucible, and allowed to dry before being fused in a furnace. Samples were optimally spiked in approximate proportions of 55 % Pt from DS and 45 % natural Pt. Where sample Pt concentrations were unknown they were estimated based on published results for similar samples. The preparation and fusion of NiS charges and dissolution of NiS beads were performed as described by Creech *et al.* (2014). Once fully digested, the samples were converted to chloride form by evaporating with concentrated HCl, and finally brought into solution in 10 mL of 0.5 M HCl for anion-exchange chemistry.

Digestion of iron meteorite samples was carried out directly by acid digestion. Small fragments of Fe–Ni metal weighing *ca.* 0.5–1.0 g were cut from larger iron meteorite specimens using a diamond cutting disc attached to a small handheld drill. Surface contamination and oxidation were removed by abrasion with fine-grained SiC sandpaper, and fragments were cleaned with ultra-pure water and methanol. The metal was then acid washed by adding *ca*. 4 mL of 1.5 M HCl at room temperature and placing it in an ultrasonic bath for a few minutes, and then by placing it in *ca*. 4 mL of 0.8 M HNO_3 on a hotplate at 120 ˚C for up to 30 min, before rinsing with ultra-pure water and drying. The Fe–Ni metal was digested in concentrated HCl or aqua regia on a hotplate at 120 ˚C. Iron meteorite samples were double-spiked prior to dissolution of the iron meteorite fragments or in an aliquot of the digested sample. Double-spike was added to have proportions of approximately 55 % of Pt from DS and 45 % natural Pt. Once fully digested and spiked, the samples were evaporated to dryness, converted to chloride form by evaporating with concentrated HCl, and finally brought into solution in 10 mL of 0.5 M HCl for anion-exchange chemistry. The sample and DS were fully equilibrated after this procedure.

Chemical separation of platinum

Purification of Pt from samples was performed using the methods described by Creech *et al.* (2014), based on separation utilising AG1-X8 (100–200 mesh) anion exchange resin. The major cationic species in rock and meteorite samples are not retained on this resin, and the platinum group elements were eluted using sequentially stronger HCl and HNO_3 acids. Pt is collected in a final step using concentrated HNO_3, with a Pt yield of ≥90 % and purity of ≥95 % (Creech *et al.*, 2014). This level of Pt separation has been shown to be adequate for accurate determination of Pt stable isotope compositions by double-spike MC-ICPMS (Creech *et al.*, 2013). All Pt separation work was conducted in class 10 laminar flow hoods situated in a class 100 clean laboratory at either Victoria University of Wellington, New Zealand, the Centre for Star and Planet Formation, Denmark, or the Institut de Physique du Globe de Paris, France. In order to destroy any

potential organic interferences, Pt cuts were treated by refluxing in aqua regia overnight on a hotplate, evaporated to dryness, and then repeatedly (n = 4 or 5) refluxed and then evaporated in HNO_3–H_2O_2 on a hotplate at 150 ˚C until no residue from the resin could be observed. Samples were then reconverted to chloride form by evaporating concentrated HCl, prior to being dissolved in 0.5 M HCl for isotopic measurement by MC-ICPMS.

Mass spectrometry (Pt)

Pt stable isotope measurements were carried out using the techniques described by Creech *et al.* (2013), using a ^{196}Pt–^{198}Pt DS to correct for instrumental mass fractionation, using ^{194}Pt, ^{195}Pt, ^{196}Pt and ^{198}Pt in the DS inversion. Isotopic measurements were made using a Nu Plasma MC-ICPMS at Victoria University of Wellington, New Zealand, or a Thermo Neptune Plus MC-ICPMS at the Centre for Star and Planet Formation, Denmark. Analytical conditions for both instruments were identical to those described by Creech *et al.* (2013). Isotope results are reported in delta notation relative to the IRMM-010 Pt isotope standard as the per mil difference in $^{198}Pt/^{194}Pt$ ratios ($\delta^{198}Pt$). Sample–spike mixtures were monitored in analyses and data points were rejected if sample–spike ratios were found to be outside the ideal range. All data reduction was conducted offline using the double-spike data reduction tool IsoSpike (Creech and Paul, 2015), which is an add-on for the Iolite data reduction package (www.iolite.org.au). IsoSpike is open-source and freely available from www.isospike.org. Pt concentrations of samples were also calculated offline using isotope dilution calculations as described by Creech *et al.* (2014).

Reproducibility of Pt isotope measurements

Individual analyses have typical internal errors (2 se) on $\delta^{198}Pt$ of *ca.* 0.020 ‰ or 0.015 ‰ for measurements made in NZ and DK, respectively. In order to monitor the long-term reproducibility of Pt stable isotope measurements, a solution standard (J. T. Baker Pt ICP solution standard) with a published Pt stable isotope composition ($\delta^{198}Pt$ = +0.09 ‰; Creech *et al.*, 2013) was employed as a secondary standard, with double-spiked analyses of the standard made in each measurement session. Repeat analyses of the Baker Pt standard have been made in three different labs, on four different MC-ICPMS instruments and over ~5 years, and yield a reproducibility of ≤0.04 ‰ (2 sd) on $\delta^{198}Pt$. Specifically during the analytical sessions represented in the data presented here, analyses of the Baker Pt standard yielded $\delta^{198}Pt_{Baker}$ = 0.09 ± 0.04 ‰ (2 sd; n = 91). Replicate samples from a homogenised powder of the carbonaceous chondrite Allende gave consistent results with a mean $\delta^{198}Pt$ = –0.12 ± 0.06 ‰ (2 sd; Table S-2). These five replicates provide the best estimate of the external reproducibility of our method for NiS processed samples, and thus error bars on all NiS processed samples in figures presented here are either the uncertainty in the weighted mean of the sample or the 2 sd of the Allende replicates (0.06 ‰), whichever is larger. The

reproducibility at lower (ppb) Pt concentrations was estimated by pooling data for the Isua suite of samples. While these are separate samples, they are formed from large degrees of partial melting from the same mantle source and therefore are expected to have a common Pt isotopic composition. Treating these eight samples as a single group (excluding one replicate of one sample (460258) as an outlier), these indicate a reproducibility of 0.07 ‰ on δ^{198}Pt. The homogeneous Pt composition defined by these samples indicates that stable Pt isotopes are robust to secondary events, as the Sm–Nd systematics in these samples (Rizo *et al.*, 2013) suggest that they have been variably affected by post-crystallisation metamorphism.

Reproducibility for iron meteorites processed by acid digestion is estimated based on three replicate digestions of Toluca (processed both in NZ and DK), which give an external reproducibility on δ^{198}Pt of ±0.05 ‰. As above, error bars in figures represent either the uncertainty in the mean of the sample or the 2 sd of the Toluca replicates (0.05 ‰), whichever is larger.

Platinum blanks

The contribution of Pt blanks was found to be consistent with those reported by Creech *et al.* (2014). Anion-exchange column Pt blanks were typically *ca.* ≤0.1 ng. The sizes of the Pt blanks introduced during sample processing were assessed by purifying Pt from multiple blank NiS digestions, and were typically *ca.* 0.5–2 ng, with an average of 0.8 ng per typical 15 g sample digestion (n = 16; Table S-3). For most samples, the effect of this amount of blank is negligible, but for exceptionally small samples or samples with extremely low Pt content (*e.g.*, <1 ng g^{-1}), the contribution from blank must be considered. Therefore, efforts were made to determine the effect of the blank on Pt isotope data and to apply a correction.

The approximate Pt isotopic composition of the blank was determined in two ways: (1) adding Pt double-spike to blank 'samples' prior to NiS digestions, and (2) adding blank to the IRMM-010 Pt isotope standard. In the former method, a number of blank NiS digestions were made and Pt double-spike was added in the proportions suggested by the average Pt blank given above. NiS beads from up to four such digestions were combined and processed in a single batch through Pt chemistry, and Pt isotopes were subsequently measured by MC-ICPMS. Given the extremely small amounts of Pt processed from these blanks, uncertainties on isotopic measurements are large (Table S-4). However, these data suggest that the composition of the Pt blank, or at least the effect of blank on the DS corrected ratios, is up to δ^{198}Pt ≈ +1.58 ‰ (Table S-4).

In the latter method, Pt blank was accumulated by combining Pt cuts from several blank NiS digestions. The blank Pt was then added to IRMM-010 Pt isotope standard in varying proportions of up to 30 % blank, and measured by MC-ICPMS (Table S-5). A regression through these data suggests a blank composition or effect of around δ^{198}Pt ≈ +1.14 ‰.

Note that both of these methods assume that, if the blank is truly fractionated, the isotopic composition of the blank is mass-dependently fractionated from a terrestrial composition.

Assuming the isotopic composition and amount of blank based on the above, a correction can be applied to the data to remove the effect of the blank. This is demonstrated using the NiS-blank-doped data described above (Table S-5; Fig. S-1).

The efficacy of this correction was also tested by taking a peridotite sample (BC-1) for which isotope data is available (Table S-1), and processing multiple replicate NiS digestions with smaller amounts (~1 g per digestion) of sample, such that the blank-to-sample ratio is significantly increased (*i.e.* up to 20 % Pt from blank). NiS beads from nine such digestions were combined into three batches for Pt chemistry and isotopic analysis (Table S-6). We found that by using the above determined blank composition (δ^{198}Ptblank = +1.58 ‰) and varying the amount of blank per digestion within the typical range of observed blank amounts (Table S-3), all of the BC-1 batch samples can be corrected to values close to those previously determined for that sample (δ^{198}Pt = –0.19 ± 0.15 ‰; Table S-6; Fig. S-1).

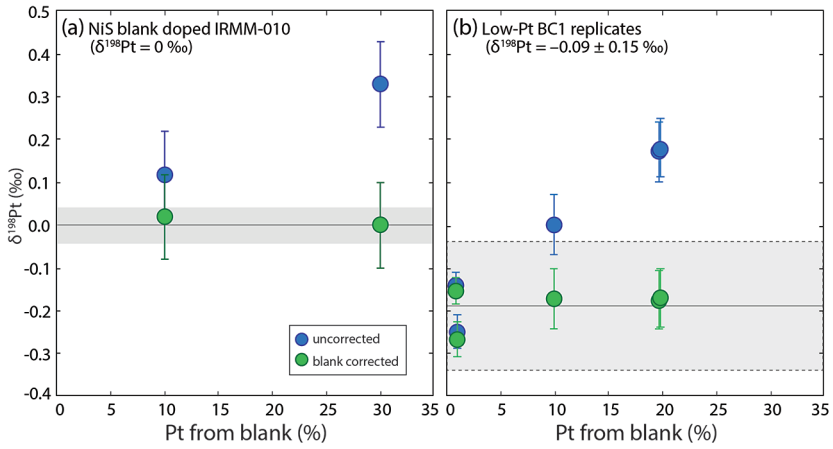

Figure S-1 Demonstration of correction for blank Pt on δ^{198}Pt data for **(a)** mixtures of blank Pt from NiS digested blanks and IRMM-010 Pt isotope standard (δ^{198}Pt = 0 ‰) and **(b)** the peridotite BC1 (δ^{198}Pt = -0.09 ± 0.15 ‰), where three samples have been prepared by combining digestions of relatively small amounts of material, thus creating a high blank-to-sample ratio. In each case, uncorrected data are shown in blue and the same data with a blank correction applied are shown in green.

Based on these results, blank corrections were calculated for the entire dataset in Tables S-1 and S-2 (with the exception of the iron meteorites, which were not digested by NiS fire assay), using the average amount of blank (0.8 ng)

per typical 15 g sample digestion and the most extreme value for the blank composition ($\delta^{198}Pt_{blank}$ = +1.58 ‰), as determined above. The size of these additional uncertainties are given in Tables S-1 and S-2 as the 'Magnitude of blank correction (‰)'. Where the proportion of Pt from blank is ≤4 %, *i.e.* for almost all samples, the correction is well within the uncertainty of the analysis. This is readily apparent in Figure 2, where extended error bars relating to the uncertainty arising from blank are very small for all but a few samples. Furthermore, in many cases, the magnitude of this correction may be overestimated due to our conservative choices of the composition and amount of blank, as described above.

Note that for samples where less than 15 g of sample were processed, the amount of sample was made up to 15 g with pure silica, and thus the amount of blank per digestion is not affected.

Model details and parameters

Modelling of terrestrial Pt isotopes as presented in Figure 3 was carried out using simple end-member mixing calculations between a hypothetical mantle composition after core formation (pre-late-veneer mantle) and a chondritic late-veneer. The Pt concentration and isotopic composition of the late-veneer are based on chondrite data presented in this work. The Pt concentration of the pre-late-veneer mantle is estimated based on published metal–silicate partition coefficients (*i.e.* $D_{Pt}^{met/sil}$), which range from ≥10^6 at low-pressure and -temperature to ~10^4 at high-pressure and -temperature (Mann *et al.*, 2012). These parameters are summarised in Table S-7.

Using these parameters, we then calculated the composition of various mixtures between these two end-members with different iterations using different hypothetical δ^{198}Pt for the pre-late-veneer mantle (Fig. 3). The only constraint on the δ^{198}Pt of pre-late-veneer mantle is to try and find some value where the mixture between pre-late-veneer mantle and late-veneer goes through the data for Isua samples as well as the post-Archean mantle composition, which assumes these samples are related by different degrees of mixing between those two end-members. This modelling shows that using the most Pt depleted pre-late-veneer mantle corresponding to core formation at low-pressure and -temperature, the Pt isotopic signature of core formation is immediately overwhelmed with a chondritic signature after the addition of minimal amounts of late-veneer, and thus the compositions of the Isua samples cannot be explained by this relationship. Conversely, assuming high-pressure and temperature core formation, the Pt concentrations and isotopic compositions in Isua samples can be explained if the pre-late-veneer mantle was fractionated to $\delta^{198}Pt \geq 4$ ‰. Further experimental or theoretical work is required to determine if Pt isotope fractionation of this magnitude is likely under these conditions. We note that the Kaapvaal samples were not used to constrain the model due to uncertainty in the origin of their Pt depletions (*i.e.* PGE data suggest that these samples have undergone melt extraction, which may have variably depleted Pt to some extent), although

the data are also consistent with this model. This could also imply that the Isua and Kaapvaal mantle sources had undergone different degrees of equilibration with late-veneer, which could relate to the relative ages of those mantle sources or spatial heterogeneity in the mixing of late-veneer into the mantle. Subsequent admixing of the remaining late-veneer inventory raised mantle Pt abundances to that observed for the PUM and shifted the post-Archean mantle Pt isotope composition to the chondritic value.

HSE and ^{187}Os analytical methods

Digestions were carried out on 1 g of whole rock powder spiked with a mixed HSE spike (^{185}Re, ^{106}Pd, ^{195}Pt, ^{191}Ir, ^{190}Os) and with 7.5 mL inverse aqua regia (2:1 HNO_3:HCl) in an Anton Paar HP-Asher at 220 °C and >100 bars for 13.5 hours. After digestion, osmium was extracted from the aqua regia solution into CCl_4 and back-extracted into HBr (Cohen and Waters, 1996) before a final purification step consisting in the micro-distillation of the Os-H_2SO_4-Cr^{6+} solution into HBr (Pearson *et al.*, 1998). After dry down, the remaining inverse aqua regia fraction was further digested at 100–120 °C using a HF/HNO_3 mixture. After equilibration in 12 N HCl, the HSE were pre-concentrated following an anion exchange chromatography procedure adapted from Pearson and Woodland (2000). Iridium, Pt, Pd and Re concentrations were analysed using the Thermo Finnigan Element 2 ICP-MS at the Steinmann Institute of the University of Bonn. Osmium concentrations and isotopic compositions (*i.e.* ^{187}Os/^{188}Os ratios) were measured using a Thermo-Finnigan Triton N-TIMS at the Department of Earth Sciences, University of Durham (UK), as described by Dale *et al.* (2008). Aliquots of the DROsS standard solution were run 4 times and are in good agreement with the values obtained by Dale *et al.* (2008) on 10–100 ng aliquots run in the Faraday mode on the same thermal ionisation mass spectrometer. Total procedural blanks are 0.72 pg Os, 0.54 pg Ir, 10.8 pg Pt, 44.1 pg Pd and 7.2 pg Re.

Supplementary Text

Platinum isotope variability amongst chondrites

Greater variability was observed amongst the eight carbonaceous chondrites analysed than in the other chondrite groups, which is thought to reflect real compositional differences that are more apparent in that group due to the greater proportions of matrix and refractory inclusions (amoeboid olivine aggregates and Ca–Al-rich inclusions). Pt usually resides inside CAI inclusions as refractory metal nuggets of nebular condensation origin as well as low-temperature Pt-Fe alloys and Fe-Ni-sulphides related to asteroidal processes (*c.f.*, Harries *et al.*, 2012; Hewins *et al.*, 2014), and these may contain Pt stable isotope or nucleosynthetic variability that is expressed in samples on this smaller scale. However, the five replicates processed from a single large homogenised sample

of Allende are identical to the mean of carbonaceous chondrites as well as that of all chondrite groups, suggesting that the chondrite reservoir that had uniform Pt stable isotope composition. The mean of all of the analysed chondrites gives the chondritic composition of $\delta^{198}Pt_{chondrite} = -0.15 \pm 0.09$ ‰ (2 sd). However, if the additional variability introduced from the smaller samples of carbonaceous chondrites is excluded, the chondritic composition can be taken as $\delta^{198}Pt_{chondrite} = -0.15 \pm 0.03$ ‰ (2 sd).

Platinum isotope variability amongst iron meteorites

Despite the relatively high concentration of Pt (typically ~5–15 μg g^{-1}) in iron meteorites, some iron meteorite samples were found to have poorer reproducibility than chondrites (Fig. S-2; Table S-2). Given the relatively large exposure ages of iron meteorites as compared to chondrites and achondrites, an obvious potential explanation for this variability between iron meteorite samples is mass independent effects arising from thermal neutron capture. The iron meteorites analysed in this study have a range of cosmic ray exposure (CRE) ages (Table S-2). Therefore, it is important to consider mass independent isotopic effects from thermal neutron capture, particularly given that the DS-corrected data in this study did not include unspiked measurements. Two recent studies have suggested using Pt isotope ratios as a dosimeter for correcting cosmogenic effects in Hf–W isotopic data (Kruijer *et al.*, 2013; Wittig *et al.*, 2013). These studies show large anomalies from production of ^{192}Pt by neutron capture on ^{191}Ir. This result partially motivated the choice of the ^{196}Pt–^{198}Pt DS used in this study, as described by Creech *et al.* (2013). Of the five stable Pt isotopes, ^{195}Pt has the largest thermal neutron capture cross section of *ca*. 28 barns (Mughabghab, 2003; Table S-8), and given the isotopes used in the ^{196}Pt–^{198}Pt DS inversion (^{194}Pt, ^{195}Pt, ^{196}Pt and ^{198}Pt), neutron capture on ^{195}Pt has the greatest potential to compromise our results.

The effect of thermal neutron capture on Pt isotope data was calculated by taking the natural relative abundances of Pt and Ir (and using a typical Pt/Ir ratio for iron meteorites), applying the mass changes from neutron captures to each isotope in proportion to its neutron capture cross section, and scaling these effects such that the anomalies produced roughly matched those published by Wittig *et al.* (2013) and Kruijer *et al.* (2013). We then estimated the sensitivity of DS corrected Pt isotope data to these effects by taking measured Pt isotope data and modifying the raw ratios by the amounts implied by these calculations. These calculations suggest that for values roughly corresponding to anomalies for Tlacotepec (the largest anomaly) in Wittig *et al.* (2013) and Kruijer *et al.* (2013), the maximum effect on DS corrected $\delta^{198}Pt$ is ~ −0.13 ‰. While this cannot be directly related to CRE ages, the effect of CRE is evidently to shift DS corrected $\delta^{198}Pt$ towards more negative compositions. As such, the apparently poor reproducibility between iron meteorites and replicate digestions of the same meteorite may in fact reflect real isotopic variations. Given that our iron meteorite data are all either chondritic or more negative than chondritic (Fig. S-2), variable

disturbance from cosmic ray exposure is the best explanation for the variability amongst these samples, especially given that the magnitude of this variability is consistent with the calculated influence described above. Cosmic ray exposure induced anomalies in W and Os isotopes have been previously shown to vary on a cm scale in iron meteorites (Leya and Masarik, 2013; Qin *et al.*, 2015). However, we emphasise that most Pt stable isotope data for iron meteorites are within error of the chondritic composition, and thus the variability discussed here has no impact on our interpretations.

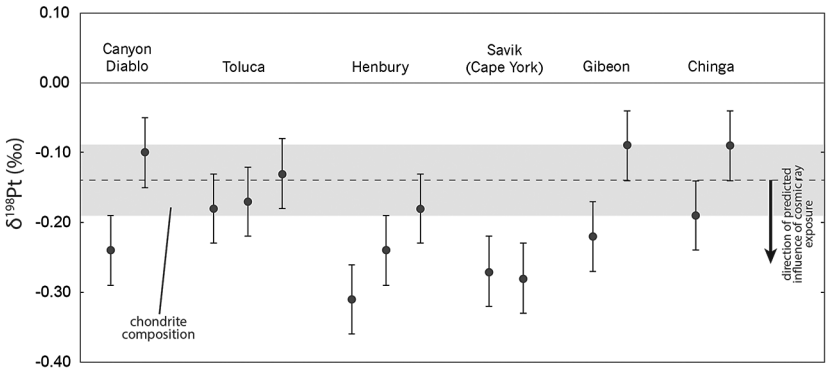

Figure S-2 Pt stable isotope data for individual replicates processed from iron meteorites. The dashed horizontal line and grey field represent the mean and 2 sd of chondrite data. The arrow indicates the expected direction of influence of cosmic ray exposure on DS-corrected Pt stable isotope data.

Platinum isotopic and abundance variations

For some sample groups, such as the Kaapvaal peridotite xenoliths, we observe isotopic variability well beyond the external reproducibility of our method. This variability is attributed to partial re-equilibration with material containing a late-veneer component. If correct, it is expected that samples with the heaviest Pt stable isotope composition should have the lowest Pt abundances. However, this correlated variability is not apparent in the Kaapvaal or Martian datasets. Considering the sizes of the samples involved, we attribute the lack of covariability to nugget effects, resulting in over- or under-estimation of Pt concentrations.

Supplementary Tables

Table S-1 Terrestrial Pt stable isotope and concentration results from double-spike MC-ICPMS, PGE concentrations from ID-ICPMS, and Re–Os isotope data determined by N-TIMS.

Sample	Rock type	Locality	Total sample processed (g)	total Pt (ng)	Pt conc. (ng g^{-1})	(n)	δ^{198}Pt (‰)	±2σ	Blank proportion (%)	Magnitude of blank correction (‰)
Subcontinental Lithospheric Mantle Xenoliths										
BC1	Lherzolite	Batchelor's Crater, Queensland, Australia	15.0	103	6.8	2	–0.25	0.04	0.8	–0.01
replicate			17.7	117	6.6	1	–0.14	0.03	0.8	–0.01
average							–0.19	0.15		
BC7	Lherzolite	Batchelor's Crater, Queensland, Australia	15.6	78	5.2	1	–0.05	0.03	1.1	–0.02
MQ1	Lherzolite	Mount Quincan, Queensland, Australia	7.2	48	6.6	1	–0.07	0.04	1.7	–0.03
MQ14	Lherzolite	Mount Quincan, Queensland, Australia	15.0	103	6.8	2	–0.17	0.03	0.8	–0.01
replicate			10.7	65	6.1	2	–0.07	0.02	1.2	–0.02
average							–0.12	0.14		
Ophiolites/transitional lherzolites										
L 213	Lherzolite	Sezia Lanzo HP zone, Alps, Italy	17.6	111	6.3	1	–0.13	0.03	0.8	–0.01
LI 138	Lherzolite	Internal Liguride Ophiolite, Italy	15.1	108	7.3	3	–0.13	0.06	0.7	–0.01
Off craton basalt-hosted xenoliths										
Mtf37	Lherzolite	Montferrier. Massif Central, France	15.1	103	6.8	3	–0.03	0.02	0.8	–0.01
Continental orogenic peridotites										
TUR 7	Lherzolite	Turon de Técouère, Pyrénées, France	16.5	119	7.2	1	–0.10	0.04	0.7	–0.01
Cratonic xenoliths (Kaapvaal craton)										
BG	Lherzolite	Kimberley, South Africa	15.0	21	1.4	2	–0.20	0.05	3.7	–0.07
BG2	Harzburgite	Kimberley, South Africa	13.1	56	4.2	2	0.16	0.03	1.4	–0.02
KBD4	Harzburgite	Kimberley, South Africa	15.3	27	1.7	2	0.27	0.06	3.0	–0.04
replicate			15.1	26	1.7	2	0.26	0.05	3.1	–0.04
replicate			15.6	30	1.9	2	0.46	0.04	2.8	–0.03
average							0.33	0.22		
LMA2	Harzburgite	Matsoku kimberlite, Lesotho	11.9	29	2.4	2	–0.08	0.04	2.8	–0.05
LTP20	Lherzolite	Thaba Putsoa kimberlite, Lesotho	7.4	4	0.6	1	0.08	0.12	18.2	–0.33
Isua										
460203	Metabasalt	Isua Supracrustal Belt, Greenland	20.25	67	3.3	3	0.13	0.09	1.6	–0.02
460204	Ultramafic schist	Isua Supracrustal Belt, Greenland	22.55	140	6.2	2	0.12	0.02	0.9	–0.01
460217	Metabasalt	Isua Supracrustal Belt, Greenland	20.58	80	3.9	1	0.16	0.16	1.4	–0.02
460218	Metabasalt	Isua Supracrustal Belt, Greenland	25.07	110	4.4	2	0.11	0.02	1.2	–0.02

Sample	Rock type	Locality		Total sample processed (g)	total Pt (ng)	Pt conc. (ng g^{-1})	(n)	δ^{198}Pt (‰)	±2σ	Blank proportion (%)	Magnitude of blank correction (‰)	
duplicate				20.69	81	3.9	1	0.07	0.07	1.4	–0.02	
average								0.09	0.05			
460219	Metabasalt	Isua Supracrustal Belt, Greenland		25.22	112	4.4	2	0.13	0.07	1.2	–0.02	
460258	Metabasalt	Isua Supracrustal Belt, Greenland		25.16	115	4.6	2	–0.08	0.06	1.2	–0.02	
duplicate				20.53	72	3.5	2	0.04	0.02	1.5	–0.02	
average								–0.02	0.17			
460275	Metabasalt	Isua Supracrustal Belt, Greenland		20.40	82	4.0	1	0.11	0.05	1.3	–0.02	
460276	Ultramafic schist	Isua Supracrustal Belt, Greenland		20.42	77	3.8	2	0.09	0.08	1.4	–0.02	

Sample	Os (ng g^{-1})	Ir (ng g^{-1})		Ru (ng g^{-1})	Pt (ng g^{-1})	Pd (ng g^{-1})	Re (ng g^{-1})	Re/Os	^{187}Os/^{188}Os	^{187}Re/^{188}Os	T_{MA} (Ma)	T_{RD} (Ma)
Subcontinental Lithospheric Mantle Xenoliths												
BC1												
BC7												
MQ1[a]	1.46						0.214			0.707	113	113
MQ14[a]	2.11						0.192			0.439	—	265
Ophiolites/transitional lherzolites												
L 213[b]	3.25	2.89		5.66	5.78	4.47	0.261			0.387		
LI 138[c]	3.04	3.06		5.45	7.15	5.95						
Off craton basalt-hosted xenoliths												
Mtf37	5.24	4.6		7.5	8.3	6.6	0.156			0.144		
Continental orogenic peridotites												
TUR 7[b]	4.03	3.59		7.22	7.2	6.54	0.341			0.408		
Cratonic xenoliths (Kaapvaal craton)												
BG	2.37	2.26		3.26	1.58	0.49	0.217	0.091	0.10661	0.43882		3091
BG2	4.59	4.45		7.01	2.72	0.06	0.023	0.005	0.10865	0.02430	2986	2823
KBD4	2.56	2.16		2.84	1.83	0.06	0.060	0.023	0.10678	0.11276	4107	3069
replicate												
replicate												
average												
LMA2	4.19	3.38		5.00	2.23	0.66	0.042	0.010	0.10724	0.04863	3376	3008
LTP20	4.42	3.15		5.79	0.44	0.08	0.170	0.039	0.10699	0.18496	5195	3041

Pt stable isotope compositions given are weighted means of the number of analyses (n) of each digestion, with the uncertainties reflecting the errors on the weighted means. Where multiple replicates were processed, the mean and 2 sd ($n \leq 2$) or weighted mean ($n \geq 3$) is also shown along with the values for each replicate. Details of analytical blanks and blank corrections are given in the Supplementary Information. All Re–Os ages for Kaapvaal samples calculated to PUM with a ^{187}Os/^{188}Os of 0.1296 and a ^{187}Re/^{188}Os of 0.435 after Becker *et al.* (2006). Model ages (TMA) for Kaapvaal samples are overestimated due to the presence of metasomatic sulphides that affect the Re/Os ratio. PGE and Re-Os data for MQ1, MQ14, L 213, LI 138, Mtf37 and TUR 7 are from the following references: [a]Handler *et al.* (2005); [b]Becker *et al.* (2006); [c]Luguet *et al.* (2004); [d]Alard *et al.* (2011).

Table S-2 Platinum stable isotope and concentration results for meteorite samples measured by double-spike MC-ICPMS.

Sample	Group	Total sample processed (g)	total Pt (μg)	Pt conc. (μg g^{-1})	Ref. Pt conc. μg g^{-1})		δ^{198}Pt (‰)	±2σ	(n)	Blank proportion (%)	Magnitude of blank correction (‰)	CRE age (Myr)	Structural type‡	Kamacite band width‡ (mm)
Ordinary chondrites														
Bovedy	L3	0.52	0.52	1.00			–0.15	0.03	3	0.2	0.00			
Begaa	LL3	0.48	0.25	0.52			–0.15	0.03	3	0.3	0.00			
Talbachat n'aït Isfoul	LL3	0.96	0.22	0.23			–0.14	0.02	4	0.4	–0.01			
replicate		0.49	0.19	0.39			–0.19	0.04	3	0.4	–0.01			
average							–0.17	0.07	7					
SAH 97172	L5	1.36	1.00	0.79			–0.16	0.04	4	0.1	0.00			
Enstatite chondrites														
SAH 97096	EH3	0.47	0.63	1.33			–0.15	0.03	4	0.1	0.00			
replicate		0.47	0.60	1.27			–0.17	0.01	1	0.1	0.00			
average							–0.16	0.03						
SAH 97159	EH3	1.24	1.47	1.12			–0.14	0.04		0.1	0.00			
Carbonaceous chondrites														
Allende	CV3	1.00	1.26	1.26	1.36		–0.10	0.04	3	0.1	0.00			
replicate		1.14	1.45	1.27			–0.10	0.07	3	0.1	0.00			
replicate		1.04	1.24	1.20			–0.13	0.01	5	0.1	0.00			
replicate		1.02	1.30	1.29			–0.12	0.04	5	0.1	0.00			
replicate		1.05	1.22	1.16			–0.17	0.02	2	0.1	0.00			
average				1.24			–0.12	0.06						
Gujba	CB3	0.48	2.13	4.42			–0.08	0.04	3	0.0	0.00			
NWA 1232	CO3	0.54	0.52	0.98			–0.08	0.03	3	0.2	0.00			
NWA 763	CO3	0.48	0.49	1.02			–0.17	0.04	3	0.2	0.00			
NWA 1559	CK3	0.66	0.32	0.49			–0.17	0.04	4	0.3	0.00			
NWA 1563	CK5	0.50	0.35	0.68			–0.08	0.03	4	0.2	0.00			
NWA 723	CV3	0.44	0.51	1.16			–0.24	0.03	3	0.2	0.00			
SaU 290	CH3	0.64	0.50	0.78			–0.16	0.03	3	0.2	0.00			
Primitive achondrites														
Dho 125	Acapulcoite	0.86	1.24	1.45			–0.09	0.02	4	0.1	0.00			
replicate		0.86	1.25	1.45			–0.09	0.02	3	0.1	0.00			
average							–0.09	0.01						
NWA 2871	Acapulcoite	0.88	1.99	2.27			–0.04	0.03	3	0.0	0.00			
Tierra Blanca	Winonaite	0.31	0.25	0.82			0.01	0.03	1	0.3	0.00			
ALH 84136	Ureilite	1.20	0.31	0.26	0.28		–0.05	0.06	3	0.3	0.00			
ALHA77257	Ureilite	1.54	0.23	0.15	0.19		–0.01	0.03	3	0.3	–0.01			
ALHA78019	Ureilite	0.27	0.25	0.90	1.54		–0.21	0.04	3	0.3	–0.01			

Sample	Group	Total sample processed (g)	total Pt (μg)	Pt conc. (μg g^{-1})	Ref. Pt conc. μg g^{-1})	δ^{198}Pt (‰)	±2σ	(n)	Blank proportion (%)	Magnitude of blank correction (‰)	CRE age (Myr)	Structural type‡	Kamacite band width‡ (mm)
ALHA81101	Ureilite	1.23	0.08	0.06	0.06	0.17	0.13	3	1.0	–0.02			
EET 87517	Ureilite	1.09	0.54	0.49	0.59	–0.05	0.06	3	0.1	0.00			
EET 96042	Ureilite	1.47	0.69	0.47	0.57	–0.04	0.06	3	0.1	0.00			
GRA 95205	Ureilite	1.00	0.54	0.54	0.83	–0.15	0.09	3	0.1	0.00			
GRA 98032	Ureilite	1.07	0.26	0.25	0.41	–0.13	0.11	3	0.3	0.00			
GRO 95575	Ureilite	1.45	0.54	0.37	0.31	0.10	0.14	3	0.1	0.00			
NWA 2234	Ureilite	0.69	0.18	0.26		0.00	0.04	4	0.4	–0.01			
PCA 82506	Ureilite	1.78	0.47	0.26	0.47	–0.19	0.02	3	0.2	0.00			
META 78008	Ureilite	0.74	0.27	0.36	1.04	–0.11	0.07	1	0.3	0.00			
Iron meteorites													
Canyon Diablo	IAB			6.09	8.0	–0.24	0.05	1			540	Og	2
replicate				6.73		–0.10	0.03	8					
average						–0.17	0.20						
Toluca	IAB			7.30	5.47	–0.18	0.03	2			600	Og	1.4
replicate				5.39		–0.17	0.05	4					
replicate				2.96		–0.13	0.02	1					
average						–0.16	0.05						
Henbury	IIIAB			15.24	18.31	–0.31	0.03	2			700	Om	0.9
replicate				16.55		–0.24	0.03	7					
replicate				15.44		–0.18	0.04	8					
average						–0.24	0.13						
Savik (Cape York)	IIIAB				11.85	–0.27	0.02	6			82	Og	1.2
replicate						–0.28	0.05	3					
average						–0.28	0.01						
Gibeon	IVA			3.90	6.91	–0.22	0.02	7			400	Of	0.3
replicate				3.90		–0.09	0.02	2					
average						–0.16	0.18						
Chinga	IVB/ung			7.61	9.56	–0.19	0.01	7			845	D	–
replicate				9.39		–0.09	0.03	7					
average						–0.14	0.14						

Pt stable isotope compositions given are weighted means of the number of analyses (n) of each digestion, with the uncertainties reflecting the errors on the weighted means. Where multiple replicates were processed, the mean and 2 sd is also shown along with the values for each replicate. Details of analytical blanks and blank corrections are given in the Supplementary Information. No blank correction was applied to iron meteorite data due to different digestion methods (Supplementary Information). Greater uncertainty in iron meteorite data may reflect cosmogenic effects in these samples, as discussed in the Supplementary Information. [§]CRE age given is weighted average for group. [a]Fischer-Gödde *et al.* (2010); [b]Rankenburg *et al.* (2008); [c]Crocket (1972); [d]Michlovich *et al.* (1994); [e]Petaev and Jacobsen (2004); [f]Scherstén *et al.* (2006); [g]Mathew and Marti (2009).

Table S-3 Determination of Pt blanks from replicate NiS blank digestions.

#	digestions	amount of 'sample' (g)	total blank (ng)	blank per 15g digestion (ng)
1	1	25.61	1.57	0.92
2	2	40.37	4.72	1.75
3	1	15.01	0.22	0.22
4	1	15.10	0.23	0.23
5	1	15.00	1.20	1.20
6	1	15.01	1.04	1.04
7	1	15.00	0.54	0.54
8	1	15.00	0.49	0.49
9	1	15.14	0.46	0.46
10	1	15.07	0.76	0.76
11	4	60.37	4.49	1.12
12	1	20.10	1.31	0.98
			mean	0.81
			median	0.84
			max	1.75

Table S-4 Isotopic composition of blanks from replicate, double-spiked, NiS blank digestions.

	Total 'sample' digested (g)	digestions	δ^{198}Pt (‰)	±	total blank (ng)	blank per 15g digestion (ng)
DS blank 1	60.37	4	0.83	0.25	4.48	1.11
DS blank 2	20.1	1	1.58	0.39	1.31	0.98

Table S-5 Pt isotope data and NiS blank correction of mixtures of IRMM-010 and NiS blank Pt.

	blank Pt proportion (%)	δ^{198}Pt (‰)	±	$\delta^{198}Pt_{BC}$ (‰)
IRMM-010	0	0.00	0.03	0.00
IRMM-010–blank mixture #1	10	0.12	0.07	0.02
IRMM-010–blank mixture #2	30	0.33	0.07	0.00

Table S-6 Pt isotope data and NiS blank correction of low-Pt replicate digestions of peridotite BC1, compared with normal digestions of the same sample.

	Total sample processed (g)	digestions	δ^{198}Pt (‰)	±	total Pt (ng)	Pt conc. (ng g^{-1})	blank per digestion (ng)	total blank (ng)	blank Pt proportion (%)	$\delta^{198}Pt_{BC}$ (‰)
BC1 low-Pt #1	2.8	3	0.17	0.07	19	6.6	1.5	4.6	20	–0.18
BC1 low-Pt #2	3.0	3	0.18	0.07	20	6.6	1.7	5.0	20	–0.17
BC1 low-Pt #3	3.2	3	0.00	0.07	18	5.6	0.7	2.0	10	–0.17
BC1	15.0	1	–0.25	0.04	103	6.8	1.0	1.0	1	–0.27
BC1	17.7	1	–0.14	0.03	117	6.6	1.0	1.0	1	–0.16

Table S-7 Model parameters used in preparing Figure 3.

Reservoir		$D_{Pt}^{met/sil}$	Pt conc. (ng g^{-1})	δ^{198}Pt (‰)
Pre-late-veneer mantle	– Low P-T	≥10^6	<1.44 x 10^{-5}	
	– High P-T	104	0.144	
Post-veneer-mantle			7.63	–0.10 ± 0.10
Late-veneer (chondrite)			982	–0.19 ± 0.14

Table S-8 Thermal neutron capture cross sections for isotopes in the mass range of platinum. [a]Isotopic abundances from Berglund and Wieser (2011). [b]Thermal neutron capture cross sections from Mughabghab (2003).

Isotope	^{190}Pt	^{191}Ir	^{192}Pt	^{193}Ir	^{194}Pt	^{195}Pt	^{196}Pt	^{197}Au	^{198}Pt
Relative abundance[a] (%)	0.01	37.27	0.78	62.73	32.97	33.83	25.24	100	7.16
Cross-section[b] (barns)	147	954	10	111	~1	28	~0.6	99	3.66

Supplementary Information References

ALARD, O., LORAND, J.-P., REISBERG, L., BODINIER, J.-L., DAUTRIA, J.-M., O'REILLY, S.Y. (2011) Volatile-rich Metasomatism in Montferrier Xenoliths (Southern France): Implications for the Abundances of Chalcophile and Highly Siderophile Elements in the Subcontinental Mantle. *Journal of Petrology* 52, 2009–2045.

BAADSGAARD, H., NUTMAN, A.P., BRIDGWATER, D., ROSING, M., MCGREGOR, V.R., ALLAART, J.H. (1984) The zircon geochronology of the Akilia association and Isua supracrustal belt, West Greenland. *Earth and Planetary Science Letters* 68, 221–228.

Becker, H., Horan, M.F., Walker, R.J., Gao, S., Lorand, J.-P., Rudnick, R.L. (2006) Highly siderophile element composition of the Earth's primitive upper mantle: Constraints from new data on peridotite massifs and xenoliths. *Geochimica et Cosmochimica Acta* 70, 4528–4550.

Berglund, M., Wieser, M.E. (2011) Isotopic compositions of the elements 2009 (IUPAC Technical Report). *Pure and Applied Chemistry* 83, 397–410.

Bodinier, J.-L., Menzies, M.A., Thirlwall, M.F. (1991) Continental to Oceanic Mantle Transition—REE and Sr-Nd Isotopic Geochemistry of the Lanzo Lherzolite Massif. *Journal of Petrology* Special Volume, 191–210.

Cohen, A.S., Waters, F.G. (1996) Separation of osmium from geological materials by solvent extraction for analysis by thermal ionisation mass spectrometry. *Analytica Chimica Acta* 332, 269–275.

Creech, J., Baker, J., Handler, M., Schiller, M., Bizzarro, M. (2013) Platinum stable isotope ratio measurements by double-spike multiple collector ICPMS. *Journal of Analytical Atomic Spectrometry* 28, 853–865.

Creech, J.B., Baker, J.A., Handler, M.R., Bizzarro, M. (2014) Platinum stable isotope analysis of geological standard reference materials by double-spike MC-ICPMS. *Chemical Geology* 363, 293–300.

Creech, J.B., Paul, B. (2015) IsoSpike: Improved Double-Spike Inversion Software. *Geostandards and Geoanalytical Research* 39, 7–15.

Crocket, J.H. (1972) Some aspects of the geochemistry of Ru, Os, Ir and Pt in iron meteorites. *Geochimica et Cosmochimica Acta* 36, 517–535.

Dale, C.W., Luguet, A., Macpherson, C.G., Pearson, D.G., Hickey-Vargas, R. (2008) Extreme platinum-group element fractionation and variable Os isotope compositions in Philippine Sea Plate basalts: Tracing mantle source heterogeneity. *Chemical Geology* 248, 213–238.

Fabriès, J., Lorand, J.-P., Bodinier, J.-L. (1998) Petrogenetic evolution of orogenic lherzolite massifs in the central and western Pyrenees. *Tectonophysics* 292, 145–167.

Fischer-Gödde, M., Becker, H., Wombacher, F. (2010) Rhodium, gold and other highly siderophile element abundances in chondritic meteorites. *Geochimica et Cosmochimica Acta* 74, 356–379.

Handler, M.R., Bennett, V.C., Carlson, R.W. (2005) Nd, Sr and Os isotope systematics in young, fertile spinel peridotite xenoliths from northern Queensland, Australia: A unique view of depleted MORB mantle? *Geochimica et Cosmochimica Acta* 69, 5747–5763.

Harries, D., Berg, T., Langenhorst, F., Palme, H. (2012) Structural clues to the origin of refractory metal alloys as condensates of the solar nebula. *Meteoritics & Planetary Science* 47, 2148–2159.

Hewins, R.H. *et al.* (2014) The Paris meteorite, the least altered CM chondrite so far. *Geochimica et Cosmochimica Acta* 124, 190–222.

Kruijer, T.S., Fischer-Gödde, M., Kleine, T., Sprung, P., Leya, I., Wieler, R. (2013) Neutron capture on Pt isotopes in iron meteorites and the Hf–W chronology of core formation in planetesimals. *Earth and Planetary Science Letters* 361, 162–172.

Leya, I., Masarik, J. (2013) Thermal neutron capture effects in radioactive and stable nuclide systems. *Meteoritics & Planetary Science* 48, 665–685.

Lorand, J.-P., Grégoire, M. (2006) Petrogenesis of base metal sulphide assemblages of some peridotites from the Kaapvaal craton (South Africa). *Contributions to Mineralogy and Petrology* 151, 521–538.

Luguet, A., Lorand, J.-P., Alard, O., Cottin, J.-Y. (2004) A multi-technique study of platinum group element systematic in some Ligurian ophiolitic peridotites, Italy. *Chemical Geology* 208, 175–194.

Mann, U., Frost, D.J., Rubie, D.C., Becker, H., Audétat, A. (2012) Partitioning of Ru, Rh, Pd, Re, Ir and Pt between liquid metal and silicate at high pressures and high temperatures - Implications for the origin of highly siderophile element concentrations in the Earth's mantle. *Geochimica et Cosmochimica Acta* 84, 593–613.

Mathew, K.J., Marti, K. (2009) Galactic cosmic ray-produced 129Xe and 131Xe excesses in troilites of the Cape York iron meteorite. *Meteoritics & Planetary Science* 44, 107–114.

Michard-Vitrac, A., Lancelot, J., Allègre, C.J., Moorbath, S. (1977) U-Pb ages on single zircons from the Early Precambrian rocks of West Greenland and the Minnesota River Valley. *Earth and Planetary Science Letters* 35, 449–453.

Michlovich, E.S., Vogt, S., Masarik, J., Reedy, R.C., Elmore, D., Lipschutz, M.E. (1994) Aluminum 26, 10Be, and 36Cl depth profiles in the Canyon Diablo iron meteorite. *Journal of Geophysical Research: Planets* 99, 23187–23194.

Mughabghab, S.F. (2003) *Thermal neutron capture cross sections resonance integrals and g-factors.* Report, INDC (NDS)-440, International Atomic Energy Agency.

Nutman, A.P., Mojzsis, S.J., Friend, C.R.L. (1997) Recognition of ≥3850 Ma water-lain sediments in West Greenland and their significance for the early Archaean Earth. *Geochimica et Cosmochimica Acta* 61, 2475–2484.

Pearson, D.G., Shirey, S.B., Harris, J.W., Carlson, R.W. (1998) Sulphide inclusions in diamonds from the Koffiefontein kimberlite, S Africa: constraints on diamond ages and mantle Re–Os systematics. *Earth and Planetary Science Letters* 160, 311–326.

Pearson, D.G., Woodland, S.J. (2000) Solvent extraction/anion exchange separation and determination of PGEs (Os, Ir, Pt, Pd, Ru) and Re-Os isotopes in geological samples by isotope dilution ICP-MS. *Chemical Geology* 165, 87–107.

Petaev, M.I., Jacobsen, S.B. (2004) Differentiation of metal-rich meteoritic parent bodies: I. Measurements of PGEs, Re, Mo, W, and Au in meteoritic Fe-Ni metal. *Meteoritics & Planetary Science* 39, 1685–1697.

Qin, L., Dauphas, N., Horan, M.F., Leya, I., Carlson, R.W. (2015) Correlated cosmogenic W and Os isotopic variations in Carbo and implications for Hf–W chronology. *Geochimica et Cosmochimica Acta* 153, 91–104.

Rankenburg, K., Humayun, M., Brandon, A.D., Herrin, J.S. (2008) Highly siderophile elements in ureilites. *Geochimica et Cosmochimica Acta* 72, 4642–4659.

Rizo, H., Boyet, M., Blichert-Toft, J., Rosing, M.T. (2013) Early mantle dynamics inferred from ^{142}Nd variations in Archean rocks from southwest Greenland. *Earth and Planetary Science Letters* 377, 324–335.

Scherstén, A., Elliott, T., Hawkesworth, C., Russell, S., Masarik, J. (2006) Hf-W evidence for rapid differentiation of iron meteorite parent bodies. *Earth and Planetary Science Letters* 241, 530–542.

Wittig, N., Humayun, M., Brandon, A.D., Huang, S., Leya, I. (2013) Coupled W–Os–Pt isotope systematics in IVB iron meteorites: In situ neutron dosimetry for W isotope chronology. *Earth and Planetary Science Letters* 361, 152–161.